Supporting Information

Step edge-mediated assembly of periodic arrays of long graphene nanoribbons on Au(111)

Chuanxu Ma, Zhongcan Xiao, Wenchang Lu, Jingsong Huang, Kunlun Hong, Jerzy Bernholc, An-Ping Li

Experimental details:

The Au(111) single crystal was cleaned by repeated cycles of Ar$^+$ sputtering and annealing at 740 K. DBBA molecules with a purity of 98.7% were degassed and then evaporated onto the Au substrate at a temperature of 470 K with one monolayer coverage. At a constant source-substrate distance and background pressure (about 2×10^{-10} torr), the source cell temperature was varied with deposition pressures of 6×10^{-9} and 2×10^{-8} torr to achieve low and high deposition rates, respectively. The sample was subsequently annealed at 470 K for 10 min and 670 K for 20 min, respectively, for polymerization and cyclodehydrogenation to form the 7-aGNRs. To grow the intermediate state, a lower graphitization temperature of 570 K was employed, similarly to previous reports.[1-3] The as-grown GNR sample was subsequently transferred from the growth chamber to the STM chamber under ultrahigh vacuum (UHV). The STM characterizations were performed with a home-made variable temperature system at 105 K with a clean commercial PtIr tip. All STM images were acquired in a constant-current mode. The bias voltage was applied to the sample bias with respect to the tip.

DFT calculation details:

The atomic structures and electronic properties of polymer assemblies on Au substrate were calculated with density functional theory (DFT). The calculations were performed with Quantum Espresso package,[4] using ultrasoft pseudopotentials[5] and

Perdew-Burke-Ernzerhof exchange-correlation functional,[6] which has a good performance in modeling metal substrate.[7] A non-local vdw-df functional[8] was used to achieve higher accuracy in the simulation of van der Waals interaction between polymer and Au,[9] which is shown to be a good choice to produce accurate adsorption energies for graphene on Au,[10] especially on substrate steps.[11] The energy cutoffs were 30 Ry and 300 Ry for the wavefunctions and charge density, respectively. The atomic structures were relaxed until forces reached a threshold of 0.002 RyÅ^{-1}. The iso-current STM images were simulated based on Tersoff's method.[12] The density isovalue is chosen to be $1e^{-5}Bohr^{-3}$ to give a consistent result with the experiment. The polymers and Au substrate were periodic in the x direction with a lattice constant of 8.64 Å, constituting two anthracene units, or one monomer, for each polymer. A k-point mesh of 5×1×1 was used for the unit cell. The step was along x direction, the distance between periodic images of the step was >40 Å. Four layers of Au atoms were used to model the substrate, with bottom layer atoms fixed. At least 20 Å vacuum spacing was used along the direction perpendicular to the substrate to decouple the periodic image effect. The adsorption energy (E_{ads}), calculated as difference of total energy and the sum of energies of two adjacent polymers in vacuum and the Au substrate, is tested for convergence against the energy cutoffs, k-point mesh and vacuum size. Note that the {100}-type step[13] normal to (110) is used in our simulations, which is consistent with our images showing that the {100}-type step is dominant in forming polymers (for example, Fig. 2).

The relation between dihedral angle and π−π stacking:

For single polymers, the dihedral angle between neighboring anthracene units remains nearly the same when they change from the adsorption on the terrace (Fig. S2a) to the adsorption on the step edge (Fig. S2b). For two assembled polymers both on the terrace (Fig. S2c), the dihedral angles for the two polymer chains are similar to those in the single polymers. The negligible change of dihedral angles is consistent with the large π−π stacking distance and the small π−π stacking interaction for the CF2-1

configuration. When they are assembled beside the step edge giving CF2-2 configuration (Fig. S2d), the dihedral angles are slightly reduced, which reflects the mediation effect of the step edge. However, the difference of the two angles is small. The dihedral angles show larger differences within the two polymer chains for CF2-3 and CF2-4 configurations with one polymer on the step while the other on the terrace (Fig. S2e,f). The largest difference of dihedral angles is observed for the CF2-4 configuration (Fig. S2f), which shows the shortest $\pi-\pi$ stacking distance and the strongest $\pi-\pi$ stacking interaction.

**The relation between dihedral angle and cyclodehydrogenation temperature:**

No direct relation is observed between dihedral angle and cyclodehydrogenation temperature. Taking single polymer chains as an example, single polymers respectively adsorbed on the terrace (Fig. S2a) and on the step edge (Fig. S2b) show similar dihedral angles. However, the cyclodehydrogenation temperatures are different, as indicated by the experimental results that the single polymers on the step edge showed an increased threshold of cyclodehydrogenation temperature (see Fig. 3b that shows intact single polymers on the step edge after 570 K annealing). This may be attributed to the strong polymer-substrate interaction when the polymers are adsorbed on the step. On the other hand, for assembled polymer arrays, one may expect a higher cyclodehydrogenation temperature for a larger dihedral angle and a lower temperature for a smaller dihedral angle, such as the two polymers adsorbed on the step and on the lower terrace in the CF2-4 configuration (Fig. S2f). Although the polymer on the lower terrace in CF2-4 shows a comparable dihedral angle to that in single polymers (Fig. S2a), an increased cyclodehydrogenation temperature is experimentally observed for both types of polymers in arrays next to step edges. This can only be explained by the enhanced $\pi-\pi$ interaction and thus steric hindrance in the compact assembly configuration.
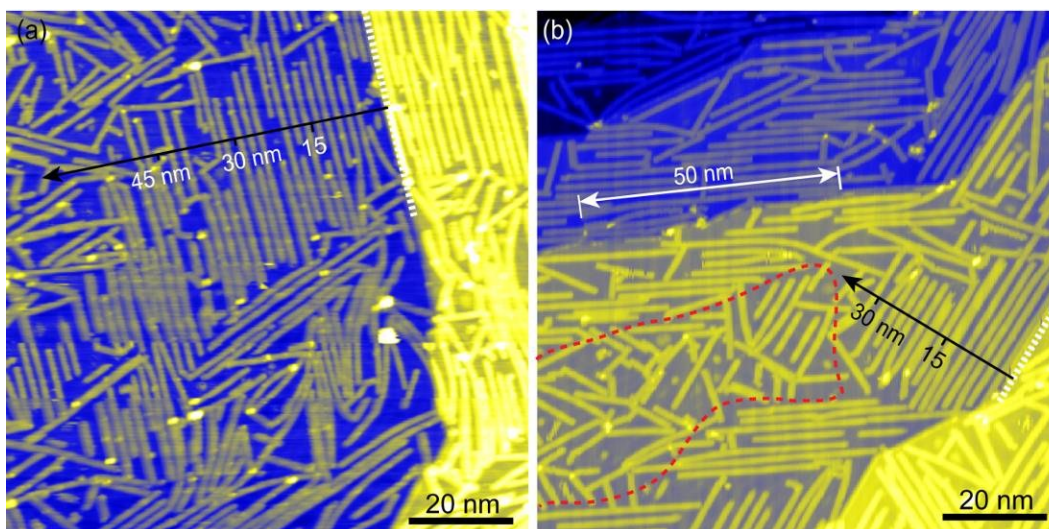
Fig. S1 (a) Large-area STM image showing well-aligned long GNRs near the straight Au step, while the GNRs become shorter and disordered at regions more than 45 nm away from the step (−2 V, 30 pA). (b) Large-area STM image showing well-aligned long GNRs on narrow terraces and regions close to Au steps, while those away from the steps are short and random (red dashed curves enclosed region) (−2 V, 30 pA). A long GNR with length of about 50 nm is marked near the Au step. A clear decrease of GNR length away from the Au step can be resolved along the black arrow. (a) and (b) are obtained with a precursor deposition pressure of 6×10^{-9} torr, the same as that for Figs. 1 and 2 in the main text.
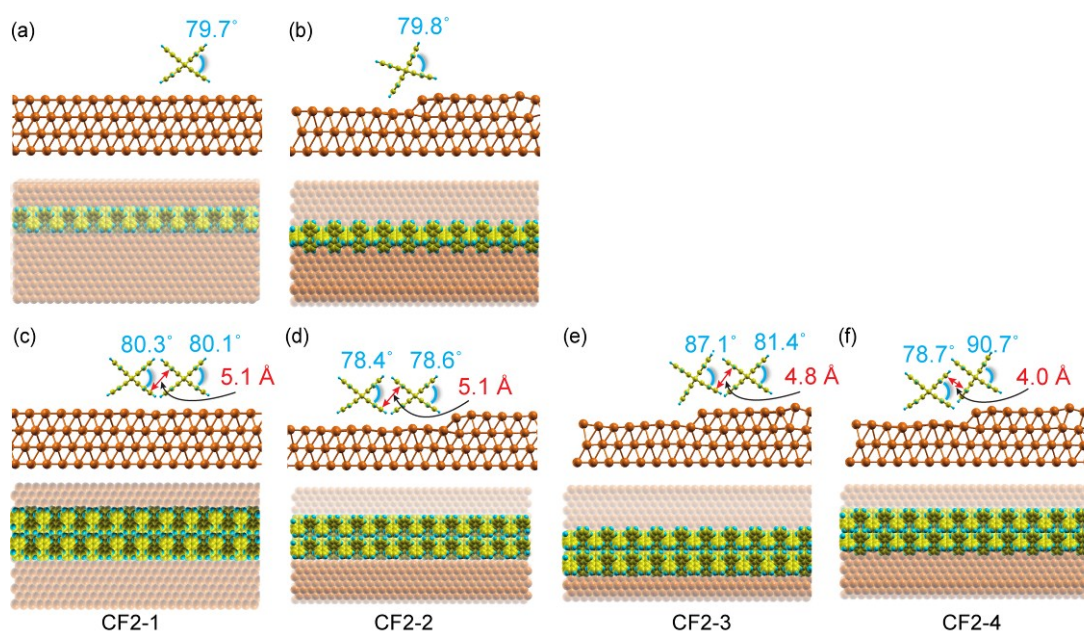
Fig. S2 (a-b) Dihedral angles between anthracene units in the single polymer chains adsorbed on the terrace and on the step edge, respectively. (c-f) Dihedral angles between anthracene units in the configurations of two assembled polymer chains, the same as those in Fig. 3h in the main text. The angles between anthracene units related to the formation of C-C bonds in the polymers are marked in each panel. The $\pi-\pi$ stacking distances in (c-f) are also shown. The top and bottom parts in each panel are the side and top views, respectively.
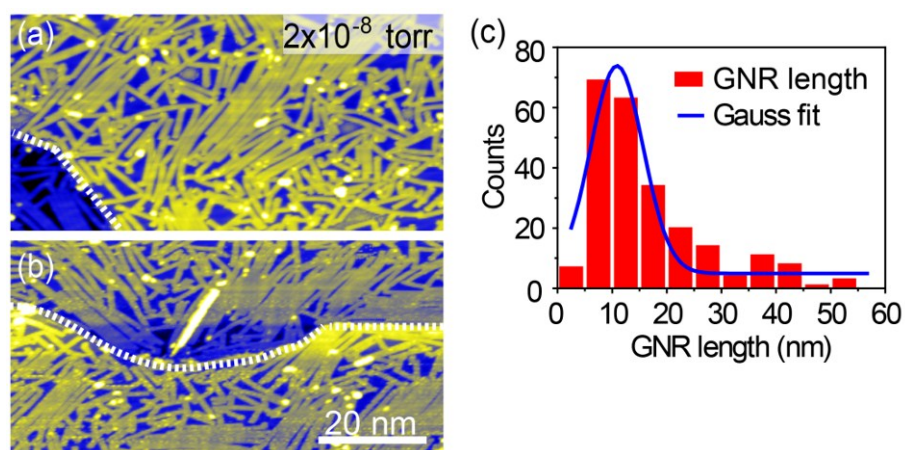
Fig. S3 (a) and (b) Two representative large-area STM images (both $80{\times}40$ nm^2) of 7-aGNRs, grown with a high precursor deposition pressure at $2{\times}10^{-8}$ torr (−3 V, 60 pA). Dashed white lines highlight the Au steps. (c) Length distribution and Gauss fit for the GNRs in (a) and (b). A mean GNR length of about 12 nm is obtained, which is much smaller than that for GNRs near the Au step (~27 nm), grown with a low precursor deposition pressure at $6{\times}10^{-9}$ torr (Figs. 1, 2 and S1). A low precursor deposition pressure corresponds to a low deposition rate, which gives enough time for molecular precursors to diffuse to and polymerize at the Au step edges, without being blocked by other polymers on the terrace, to achieve well aligned long polymers.
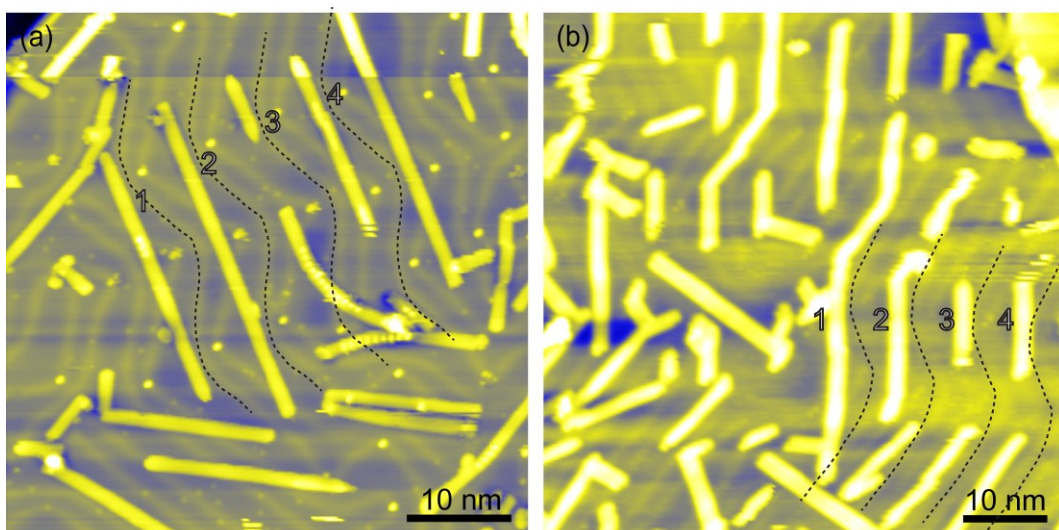
Fig. S4 (a) and (b) Two representative large-area STM images of low-coverage 7-aGNRs. Setpoint in (a): −2 V, 100 pA; Setpoint in (b): −2 V, 20 pA. Both in (a) and (b), labels 1-4 are provided next to four GNRs growing in parallel and nearly equally separated along the zigzag-patterned (22× √3) herringbone reconstruction, which are similar to previously reported observations.[14]

Supplementary References:

1. S. Blankenburg, J. Cai, P. Ruffieux, R. Jaafar, D. Passerone, X. Feng, K. Müllen, R. Fasel and C. A. Pignedoli, *ACS Nano*, 2012, **6**, 2020-2025.

2. C. Ma, Z. Xiao, J. Huang, L. Liang, W. Lu, K. Hong, B. G. Sumpter, J. Bernholc and A.-P. Li, *Phys. Rev. Materials*, 2019, **3**, 016001.

3. Z. Xiao, C. Ma, J. Huang, L. Liang, W. Lu, K. Hong, B. G. Sumpter, A. P. Li and J. Bernholc, *Adv. Theory Simul.*, 2018, **2**, 1800172.

4. P. Giannozzi, S. Baroni, N. Bonini, M. Calandra, R. Car, C. Cavazzoni, D. Ceresoli, G. L. Chiarotti, M. Cococcioni, I. Dabo, A. D. Corso, S. de Gironcoli, S. Fabris, G. Fratesi, R. Gebauer, U. Gerstmann, C. Gougoussis, A. Kokalj, M. Lazzeri, L. Martin-Samos, N. Marzari, F. Mauri, R. Mazzarello, S. Paolini, A. Pasquarello, L. Paulatto, C. Sbraccia, S. Scandolo, G. Sclauzero, A. P. Seitsonen, A. Smogunov, P. Umari and R. M. Wentzcovitch, *J. Phys.: Condens. Matter.*, 2009, **21**, 395502.

5. D. Vanderbilt, *Phys. Rev. B*, 1990, **41**, 7892-7895.

6. J. P. Perdew, M. Ernzerhof and K. Burke, *J. Chem. Phys.*, 1996, **105**, 9982-9985.

7. L. Vega, J. Ruvireta, F. Viñes and F. Illas, *J. Chem. Theory Comput.*, 2018, **14**, 395-403.

8. T. Thonhauser, V. R. Cooper, S. Li, A. Puzder, P. Hyldgaard and D. C. Langreth, *Phys. Rev. B*, 2007, **76**, 125112.

9. Z. Xiao, C. Ma, W. Lu, J. Huang, L. Liang, K. Hong, A.-P. Li, B. G. Sumpter and J. Bernholc, *npj Comput. Mater.*, 2019, DOI: 10.1038/s41524-019-0228-6.

10. H. Muñoz-Galán, F. Viñes, J. Gebhardt, A. Görling and F. Illas, *Theor. Chem. Acc.*, 2016, **135**, 165.

11. S. González, F. Viñes, J. F. García, Y. Erazo and F. Illas, *Surf. Sci.*, 2014, **625**, 64-68.

12. J. Tersoff and D. R. Hamann, *Phys. Rev. B*, 1985, **31**, 805-813.

13. S. Rousset, V. Repain, G. Baudot, Y. Garreau and J. Lecoeur, *J. Phys.: Condens. Matter.*, 2003, **15**, S3363-S3392.

14. C. Moreno, M. Paradinas, M. Vilas-Varela, M. Panighel, G. Ceballos, D. Peña and A. Mugarza, *Chem. Commun.*, 2018, **54**, 9402-9405.